Analyst

Accepted Manuscript

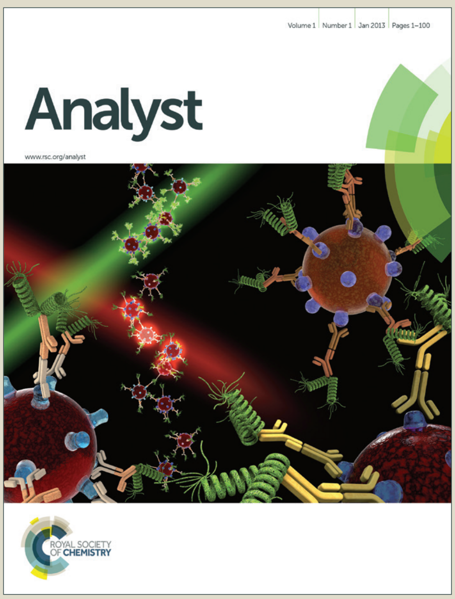

ROYAL SOCIETY OF CHEMISTRY

www.rsc.org/analyst

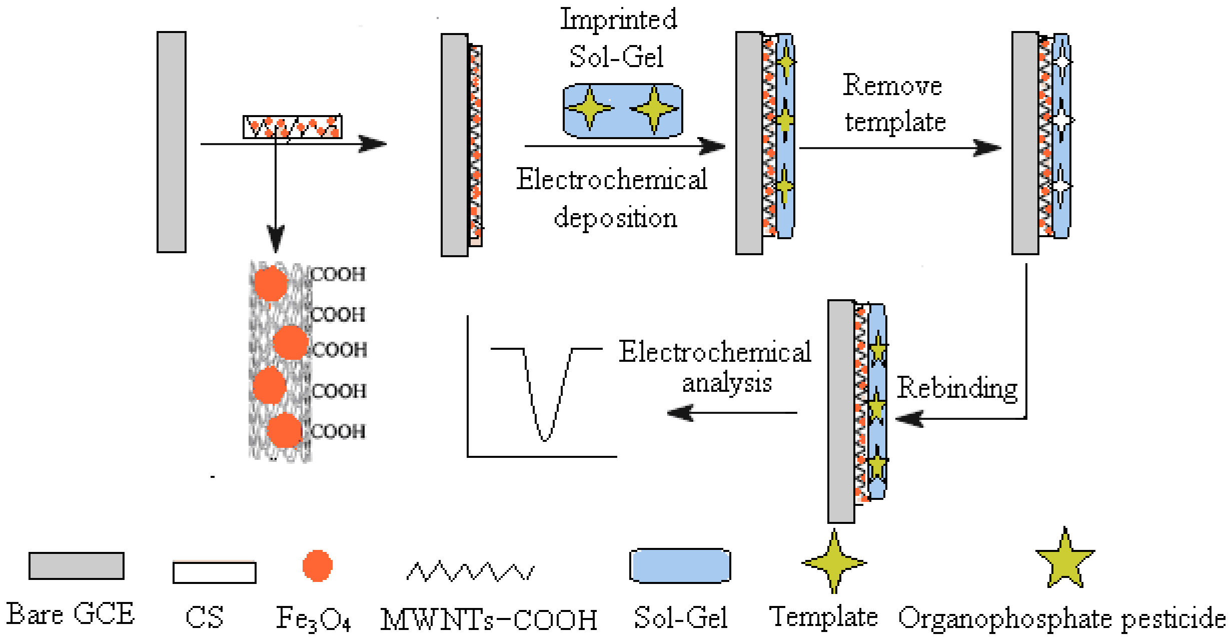

Graphic for manuscript

Development of molecularly imprinted electrochemical sensors based on Fe_3O_4@MWNTs-COOH/CS nanocomposite layers for detecting traces of acephate and trichlorfon

Qinghua Tang,[a] Xiujuan Shi,[a] Xiaolin Hou,[a] Jie Zhou[b] and Zhixiang Xu*[a]

[a]*College of Food Science and Engineering, Shandong Agricultural University, Tai'an 271018, China*

[b]*College of Chemistry and Material Science, Shandong Agricultural University, Tai'an 271018, China*

*Corresponding author. Tel.: +86 538 8246021; fax: +86 538 8242850. *E-mail address*: zhixiangxu@sina.com (Z. X. Xu).

Abstract

In this study, we developed a novel biomimetic electrochemical sensor sensitized with Fe_3O_4@carboxyl-functionalized multiwalled carbon nanotubes/chitosan nanocomposite layer using molecularly imprinted film as recognition element for the rapid detection of acephate and trichlorfon. The performance of the imprinted sensor was investigated using cyclic voltammetry and differential pulse voltammetry, and results indicated that the sensor exhibited fast responses to both acephate and trichlorfon. The imprinted sensor had good linear current responses to acephate and trichlorfon concentrations in the ranges from 1.0×10^{-4} to 1.0×10^{-10} M and 1.0×10^{-5} to 1.0×10^{-11} M, respectively. Under optimal conditions, the imprinted sensor had low limits of detection (signal to noise, S/N=3) of 6.81×10^{-11} M for acephate and 8.94×10^{-12} M for trichlorfon. The developed method was successfully applied to detect the acephate and trichlorfon spiked in the fortified kidney bean and cucumber samples with good recoveries ranging from 85.7% to 94.9% and relative standard deviations of 3.46–5.18%.

***Keywords*:** Electrochemical sensor; Molecular imprinting; Imprinted film; Fe_3O_4@MWNTs-COOH; Chitosan; Multi-pesticide residues

Introduction

Organophosphate pesticides (OPs) are extremely effective at killing destructive insects and have played an important role in increasing agricultural productivity.[1] Although OPs are highly effective in pest control, they degrade easily and do not tend to accumulate in living organisms. However, they are readily absorbed through the skin and respiratory tract, risking the health of humans and animals.[2, 3] To date, a large number of methods, including gas/liquid chromatography,[4-7] gas chromatography or liquid chromatography coupled with mass spectrometry,[8-11] fluorimetry,[12] capillary electrophoresis[13] and surface plasmon resonance[14] have been developed to detect OPs. These techniques have shown high precision for the quantitative detection of OPs. However, applications of these techniques are limited because the instruments are expensive and complicated to operate. The development of a convenient, rapid, reliable and low-cost method for detecting trace levels of OPs in food is desirable.

Electrochemical sensors (such as voltammetric, potentiometric, conductometric and capacitance sensors) are becoming important tools in medical, biological and environmental analysis because of their simplicity, high sensitivity and they are relatively inexpensive.[15] Recently, many electrochemical sensors based on molecularly imprinted polymers (MIPs) have been reported.[16-18] Compared with the biological receptors for biological antibodies, molecularly imprinted materials possess many advantages such as high stability, and they can easily be adapted for different compounds with specific binding sites.[19] Although the use of MIPs as sensing materials has expanded the field of sensor applications, many shortcomings such as the low mass transfer rate still exist.[20] Sol-gel process is a promising way to improve the performance of MIPs.[21] An inorganic framework is formed around a suitable template via non-covalent/covalent interactions among the functional monomers and the template in the sol-gel process.[22] Therefore, the combination of molecular imprinting technology and a sol-gel process is an appropriate way to construct electrochemical sensing devices. However, low sensitivity still exists in application of the MIP sensors, and the diffusion of analytes across the MIP film needs to be accelerated to obtain a quick response. To overcome these shortcomings, an appropriate sensing medium for the electron transfer and the electrocatalyst is required to enhance the sensitivity of the electrochemical detection.

Over the past decade, great efforts have been made using multiwalled carbon nanotubes (MWNTs) as a sensing medium.[23] MWNTs can enhance the sensitivity of the electrochemical detection because of their attractive electronic, chemical and mechanical properties.[24-27] Compared with MWNTs, carboxyl-functionalized multiwalled carbon nanotubes (MWNTs-COOH) have better dispersion and stability.[22] At the meantime, Fe_3O_4 is a type of magnetic nanoparticle that is environmentally friendly, low cost, easy to prepare and possesses excellent water solubility. In addition, Fe_3O_4 exhibits good electrical properties owing to the electron transfer between Fe^{2+} and Fe^{3+}.[28] Therefore, coupling MWNTs-COOH with Fe_3O_4 as the sensing medium can improve the electron transfer and electrocatalyst and enhance the detection sensitivity of electrochemical sensors. The resulting Fe_3O_4@MWNTs-COOH nanocomposite brings new capabilities for electrochemical sensing due to the synergetic effect between Fe_3O_4 and MWNTs-COOH. Chitosan (CS) is a polysaccharide, derived from the deacetylation of chitin[29] and has been widely used as an electrode modification material. Compared with some traditional dispersants such as N,N-dimethylformamide and dihexadecyl hydrogen phosphate, CS is a promising material[30] because of its attractive characteristics involving its film-forming ability, high mechanical strength, adhesion and biocompatibility.[31] Thus, CS was chosen as the dispersant for the Fe_3O_4@MWNTs-COOH nanocomposite in this study to overcome the drawbacks of some traditional dispersants.

MIPs prepared using traditional methods can only selectively recognize the template and their adsorption capacities toward other analytes are low. Thus, their applications in multi-residue analysis are limited. 4-(Dimethoxyphosphorothioylamino)butanoic acid has common functional groups and the structure of OPs and has been used as the hapten to immunize animals to obtain antibodies that can selectively recognize multi-pesticides.[32] In this study, a MIP film that can selectively recognize acephate and trichlorfon was prepared by molecular imprinting technology combined with sol-gel process using 4-(dimethoxyphosphorothioylamino)butanoic acid as the template molecule. Using the MIP film sensitized with Fe_3O_4@MWNTs-COOH/CS as recognition element, a biomimetic sensor will be developed. The effect of Fe_3O_4@MWNTs-COOH/CS nanocomposites on the performance of the imprinted film were investigated using cyclic voltammetry (CV) and differential pulse voltammetry (DPV) measurements. The factors that affected the detection sensitivity of the method are discussed in detail. The accuracy and applicability of the method are also evaluated. This research aimed to overcome the existing shortcomings of the long response time, poor signal stability and recognition of multi-pesticides with the MIP sensor and offer a sensitive, stable and accurate electrochemical sensor that can detect acephate and trichlorfon.

Experimental

Materials

The organic kidney bean and cucumber samples were purchased from Taishan Yaxiya Food Co., Ltd. (Tai'an, China) in April 2014.

Reagents

Acephate, trichlorfon, methamidophos and omethoate were obtained from the Institute for the Control of Agrochemicals, Ministry of Agriculture (Beijing, China) with purities all above 99%. CS (90%) was obtained from Shanghai Yuanye Biotechnology Co., Ltd. (Taizhou, China). MWNTs with purity over 95% were obtained from Beijing Nachen Technology Co., Ltd. (Beijing, China). O,o-dimethyl phosphorochloridothioate was purchased from Sigma-Aldrich Co., Ltd. 4-Aminobutyric acid was purchased from TCI Development Corp. (Shanghai, China). 3-Aminopropyltriethoxysilane (APTES) and tetraethoxysilane (TEOS) were obtained from WD Silicone Co., Ltd. (Wuhan, China). Tetrahydrofuran, ferric chloride ($FeCl_3$) and iron (II) chloride tetrahydrate ($FeCl_2 \cdot 4H_2O$) were obtained from Tianjin Bodi Chemical Co., Ltd (Tianjin, China). The ammonia solution (25%) was purchased from Kaitong Chemical Reagents Co., Ltd. (Tianjin, China). Ethyl acetate was obtained from Yongda Chemical Reagents Co., Ltd. (Tianjin, China). Phosphate-buffered solutions (PBSs) with various pH values were prepared with 0.2 M of H_3PO_4, 0.2 M of NaH_2PO_4 and 0.2 M of Na_2HPO_4 and their pH was then adjusted by adding either 1.0 M of HCl or 1.0 M of NaOH. The supporting electrolyte was made of 0.2 M of PBS containing 0.2 M of KCl. The oxidation-reduction probe solution (ORPS) was made of 2.0 mM of $K_3Fe(CN)_6/K_4Fe(CN)_6$ (1:1, mol/mol) in the supporting electrolyte (pH=7.0).

Instruments and apparatus

The CV and DPV experiments were performed with a CHI 620D electrochemical workstation (CH Instrument Company, Shanghai, China). All of the electrochemical experiments were performed with a conventional three-electrode system consisting of a bare or modified glassy carbon electrode (GCE) (4.0 mm in diameter) as the working electrode, a saturated calomel electrode as the reference electrode and a platinum sheet as the counter electrode. X-ray diffraction (XRD) measurements were carried out using a D8-advance diffractometer (Bruker, Germany). The fourier transform infrared (FT-IR) spectra (4000–400 cm^{-1}) with KBr was recorded using a Vector 22 spectrometer (Bruker, Germany). Transmission electron microscopy (TEM) images were recorded using a Tecnai 20U-TWIN microscope (Philips, Netherlands).

Analysis of the OPs was performed using a 2010 GC (Shimadzu, Kyoto, Japan) equipped with a flame photometric detector and a PC-based data system. The separation was conducted in a Rtx-1 capillary column (30 m × 250 μm internal diameter × 0.1 μm film thickness). Nitrogen was used as the carrier gas at a constant flow rate of 1.0 mL min^{-1} with an injection volume of 1.0 μL. The injection port temperature was held at 180 °C at the split mode with a split ratio of 4:1. The temperature of the detector was held at 270 °C. The oven temperature was programmed as follows: the temperature was held at 50 °C for 1.0 min and then it was increased to 200 °C at a rate of 15 °C min^{-1} where it was held for 1 min. After that, the temperature was increased to 220 °C at a rate of 2 °C. Finally, the temperature was raised to 240 °C at 20 °C min^{-1} and maintained for 5 min.

Synthesis of the 4-(dimethoxyphosphorothioylamino)butanoic acid

4-(Dimethoxyphosphorothioylamino)butanoic acid was synthesized according to the method reported by Zhang et al.[32] First, 0.103 g of 4-aminobutyric acid was dissolved in 10 mL of NaOH (2.5 M). After stirring for 30 min in an ice bath, 1.215 mL of o,o-dimethyl phosphorochloridothioate was added. Then, 2.5 M of NaOH was added drop-wise into the solution until the pH reached 10. After stirring for another 6 h at room temperature (RT), the mixture was washed with ethyl acetate to remove any impurities and then the pH of the reaction solution was adjusted to 2.0 by adding 1.0 M of HCl. Finally, the mixture was extracted with ethyl acetate (3×25 mL) and the organic layers were combined and dried with Na_2SO_4. The final product was obtained by rotary evaporation.

Preparation of the MIP/Fe_3O_4@MWNTs-COOH/CS/GCE

Initially, MWNTs-COOH were prepared according to the method reported by Zhang et al.[33] An amount of 500 mg of MWNTs was added to a 60 mL solution of H_2SO_4/HNO_3 (3:1, v/v) and the mixture was ultrasonicated for 15 min. Then, the mixture was stirred at 85 °C for 12 h. After cooling to RT, the product was isolated by filtration through a 0.22 μm polycarbonate membrane and washed with doubly deionised water (DDW) several times until the pH of the filtrate was neutral. Finally, the resulting MWNTs-COOH was dried under vacuum at 40 °C for 12 h.

Fe_3O_4@MWNTs-COOH nanocomposites were prepared according to the method described previously by Kong et al.[34] 20.0 mg of the MWNTs-COOH was dissolved in 20.0 mL of DDW and was ultrasonicated for 15 min. Then, 23.3 mg of $FeCl_3 \cdot 6H_2O$ was added. After the mixture was stirred vigorously for 30 min under a N_2 atmosphere, 10.0 mg of $FeCl_2 \cdot 4H_2O$ was added and the solution was kept stirring for another 30 min. Afterwards, 10 mL of a 5% ammonia solution was slowly added to the mixture. The solution was then heated to 60 °C for 2 h, and the whole preparation procedure was under a N_2 atmosphere. The relevant chemical reactions are expressed as:

$Fe^{2+} + 2Fe^{3+} + 8OH^- +$ MWNTs-COOH $\rightarrow Fe_3O_4$@MWNTs-COOH $+ 4H_2O$.

The reaction mixture was then centrifuged and washed with ethanol and DDW. Finally, the product was dried under a vacuum oven at 40 °C for 12 h and then stored at 4 °C for further use.

Fe_3O_4@MWNTs-COOH/CS/GCE was fabricated as follows: Prior to coating, the bare GCE was polished with 0.05 μm alumina slurry, followed by thoroughly flushed with DDW. It was then ultrasonically cleaned in 10 mL of nitric acid (1:1, v/v), followed by ethanol and DDW for 3.0 min each. Fe_3O_4@MWNTs-COOH (3.0 mg) and CS-acetic acid solution (1.0 wt%, 1.0 mL) were mixed in a centrifuge tube and ultrasonicated for 20 min to form a homogeneous Fe_3O_4@MWNTs-COOH/CS suspension solution. Then, the bare GCE was coated with 10.0 μL of Fe_3O_4@MWNTs-COOH/CS suspension solution and slowly dried at RT. MWNTs-COOH/CS/GCE, Fe_3O_4/CS/GCE and CS/GCE were prepared by coating 10.0 μL of MWNTs-COOH/CS dispersion (3.0 mg mL^{-1}), Fe_3O_4/CS dispersion (3.0 mg mL^{-1}) and CS/acetic acid solution on the GCE surfaces, respectively.

The MIP film was prepared on Fe_3O_4@MWNTs-COOH/CS/GCE using a sol-gel technology (Fig.

1). Firstly, 0.1515 g of 4-(dimethoxyphosphorothioylamino)butanoic acid (1.33 mmol) and 0.47 mL of APTES (2.0 mmol) were dissolved in 5.0 mL of tetrahydrofuran under magnetically stirring for 15min, following the addition of 0.59 mL of TEOS (2.66 mmol). After adding 0.15 mL of an ammonia solution (0.1 M) for another 15 min, the mixture solution was then stirred for another 2 h. Finally, the MIP/Fe_3O_4@MWNTs-COOH/CS sensor was fabricated by electrochemical deposition using CV for 10 cycles with the above mixture solution, where the potential ranged from −0.4 to +0.8 V and the scan rate was 50 mV s^{-1}. The decorated electrode was left to dry overnight at RT. The resulting electrode was suspended in 20 mL of methanol and acetic acid (9:1, v/v) and was stirred magnetically for 2 h to remove the template. Then, the modified electrode was rinsed with DDW and left to dry at RT for 24 h.

The non-imprinted polymer (NIP)/Fe_3O_4@MWNTs-COOH/CS/GCE was also prepared by using an identical procedure, without the addition of the template.

Electrochemical measurements

Electrochemical measurements were performed using CV and DPV and were carried out with a three-electrode system. The CV was scanned from −0.2 V to +0.6 V at a rate of 50 mVs^{-1}. DPV was performed in the potential range between 0 and +0.5 V with an amplitude of 0.025 V and a step potential of 0.05 V.

An initial peak current (i_0) of the DPV was recorded when the imprinted electrode was immersed in the ORPS. The imprinted electrode was then incubated in different concentrations of acephate, trichlorfon solutions or a sample solution, washed by DDW carefully and dried under nitrogen. Afterwards, the imprinted sensor was immersed in the ORPS and the peak DPV current (I_x) was re-recorded. The sensor response was obtained from the change in the reduction current of the ORPS and was calculated from the difference between I_0 and I_x ($\Delta I = I_x - I_0$). Finally, the imprinted sensor was stirred magnetically in a methanol/acetic acid (9:1, v/v) solution for 2 h to prepare for the next analysis.

Sample preparation

To investigate the applicability and accuracy of the MIP/Fe_3O_4@MWNTs-COOH/CS sensors, the fortified kidney bean and cucumber samples were prepared and it was verified that they were free of OPs using the GC method before they were spiked. Samples (2.0 g) of the fortified kidney bean and cucumber were cut into pieces and separately weighed into 100 mL conical flasks. The kidney bean and cucumber samples were spiked with either acephate (3.0×10^{-10}, 1.5×10^{-9} and 3.0×10^{-9} M) or trichlorfon (4.0×10^{-11}, 2.0×10^{-10} and 4.0×10^{-10} M) standard solutions, respectively with three different concentrations. After they were incubated for 4 h, the spiked samples were ultrasonicated with 3×10 mL of PBS (the pH was 5.5 for acephate and 7.5 for trichlorfon) for 30 min. The extractions were collected in 50 mL flasks separately and diluted to 50 mL with PBS. The resulting filtrates were filtered through a 0.45 μm membrane and were analyzed with the MIP sensor and the electrochemical responses were recorded.

Results and discussion

Characterization of Fe_3O_4@MWNTs-COOH

MWNTs-COOH and Fe_3O_4@MWNTs-COOH were analyzed by FT-IR spectroscopy. Fig. S1 showed the characteristic peaks at 3440 cm^{-1} and 1640 cm^{-1} of the stretching vibrations, which were ascribed to the O–H and C=O in the carboxylic groups (COOH), respectively.[35] The broad band at 573 cm^{-1} was from the stretching vibration of Fe–O–Fe (Fig. S1 b) in Fe_3O_4.[36] In addition, the peaks at 1375 cm^{-1} and 1368 cm^{-1} corresponding to C–C stretching originated from the MWNTs.[37]

The XRD patterns indicated that the crystal structures of the materials were composed of MWNTs and MWNTs-COOH and diffraction peaks at 2θ=26.1° were observed (Fig. 2(A)), which is consistent with previous reports.[38, 39] The XRD pattern for MWNTs-COOH (Fig. 2(A) b) was similar to that of the MWNTs (Fig. 2(A) a). However, for MWNTs-COOH, the diffraction peaks had higher intensities and the crystallization peaks were more dominant. One possible reason is that the acidification of the MWNTs advanced removing the amorphous carbon, carbon nanoparticles and metal particles. Diffraction peaks for Fe_3O_4 at 2θ values of 30.58 °, 35.56 °, 43.32 °, 53.75 °, 57.27° and 62.77° were assigned to the (220), (311), (400), (422), (511) and (440) crystal planes in Fe_3O_4 (Fig. 2(B) d), respectively, which agreed with the reported values.[40] A diffraction peak at 2θ=26.1° appeared (Fig. 2(B) c). Thus, the graphitic structure of MWNTs-COOH was not destroyed after they were coated with Fe_3O_4 nanoparticles.

TEM was used to characterize the microstructures of MWNTs-COOH and Fe_3O_4@MWNTs-COOH nanocomposite (Fig. 3). Fig. 3b revealed that the Fe_3O_4 nanoparticles were coated on the surface of MWNTs-COOH, which confirmed the formation of Fe_3O_4@MWNTs-COOH nanocomposite instead of the physical mixture of the two components.

Based on the above results, it can be concluded that Fe_3O_4@MWNTs-COOH nanocomposites were successfully synthesized.

Preparation of MIP/Fe_3O_4@MWNTs-COOH/CS/GCE

In this study, APTES was employed as the functional monomer because its amino groups could interact with the template molecules 4-(dimethoxyphosphorothioylamino)butanoic acid. TEOS acted as a cross-linker to form the polymeric network through Si–O bonds via hydrolysis. CV was employed to electrodeposit the imprinted film on the surface of the Fe_3O_4@MWNTs-COOH/CS/GCE (Fig. 4). Results indicated that the template was not electrochemically oxidized and reducted in the potential range of the electrodeposition, suggesting that the template remained unchanged during the electrodeposition process. In addition, the thickness of the imprinted film could easily be controlled by varying the number of scanning cycles during the electrodeposition process. When the scanning time was increased from 1 to 10 cycles, the width of the current decreased by about 5 μA because of the insulation of the imprinted film. After scanning for 10 cycles, the current density changed slightly. Thus, the optimum CV scanning cycle of 10 cycles was selected to form a proper imprinted layer on the surface of the Fe_3O_4@MWNTs-COOH/CS/GCE.

Electrochemical characterization

CV and DPV were effective and convenient techniques for probing the features of the imprinted sensors. Fig. 5(A) showed a comparison of the CV measurements for different modified electrodes. The bare GCE showed a pair of redox peaks (Fig. 5(A) a). Compared with the bare GCE, the peak current of CS/GCE decreased because CS increased the electrical resistance of the electrode (Fig. 5(A) b). Nonetheless, CS was chosen as the electrode modification material because of its excellent characteristics including its film-forming ability and adhesion. When the electrode surface was coated with a Fe_3O_4@MWNTs-COOH/CS nanocomposite film, the redox peak current of the CV increased (Fig. 5(A) e) and was higher than that of Fe_3O_4/CS/GCE (Fig. 5(A) c) and MWNTs-COOH/CS/GCE (Fig. 5(A) d), indicating that Fe_3O_4 and MWNTs-COOH effectively improved the current response because of their synergetic effect. Fig. 5(A) f showed the CV of MIP/Fe_3O_4@ MWNTs-COOH /CS/GCE before the template had been removed. Compared with the peak current in the Fe_3O_4@MWNTs-COOH/CS/GCE (Fig. 5(A) e), the peak current in Fig. 5(A) f was obviously reduced. This was attributed to the modification of the MIP film. After the template was removed (Fig. 5(A) g), an increase in the peak current was observed. This might be because some of the cavities enhanced the diffusion of $K_3Fe(CN)_6$/$K_4Fe(CN)_6$ through the MIP film and accelerated the redox reaction.

Fig. 5(B) showed the DPV responses of the modified sensor under different conditions. Before extracting the template, there was almost no reductive peak (Fig. 5(B) h) because the imprinted film on the Fe_3O_4@MWNTs-COOH/CS/GCE was insulating. The reductive peak current was obviously increased (Fig. 5(B) i), revealing that the template had almost been removed. After the MIP/Fe_3O_4@MWNTs-COOH/CS/GCE was incubated in 1.0 mM of acephate or trichlorfon solution, the reductive peaks were obviously reduced (Fig. 5(B) j and k), which indicated that the imprinted sensor had good affinity ability for acephate and trichlorfon. However, there was little electrochemical response with NIP/Fe_3O_4@MWNTs-COOH/CS/GCE because the film was dense and did not have imprinted cavities (Fig. 5(B) l).

The electrochemical mechanism can usually be obtained from the relationship between the peak current and the scan rate. The CV curves of the imprinted sensors in the ORPS at different scan rates were investigated in the range, 10–250 mV s^{-1}. As seen in Fig. S2, the peak currents of the CV in the imprinted sensor increased with the increment of the scan rate. The anodic (I_{pa}) and cathodic (I_{pc}) peak currents were nearly independent of the scan rate and can be expressed as: I_{pa} (mA)=−0.0698+0.0435$\upsilon^{1/2}$ (R^2=0.9988) and I_{pc} (mA)=0.0707−0.043$\upsilon^{1/2}$ (R^2=0.9980) (where υ is the scan rate with units mV s^{-1}), suggesting typical surface controlled electrochemical behavior.

Optimization of the experimental conditions

The influences of the pH of PBS on the current responses for acephate and trichlorfon were examined by DPV in the ranges from 4.0 to 7.0 and 5.5 to 8.5, respectively (Fig. S3). The △I gradually increased with an increasing pH and then decreased as the pH exceeded 5.5 for acephate and 7.5 for trichlorfon. Therefore, maximum responses for acephate and trichlorfon were observed at pH values of 5.5 and 7.5, respectively, which were selected for further investigations.

The incubation time is another critical factor that affects the performance of the imprinted sensors.[1] In this study, the incubation times of the MIP sensor for acephate and trichlorfon were evaluated from 5 to 40 min and 1 to 15 min, respectively. As shown in Fig. S4, the responses reached a plateau after incubation times of 20 min and 5 min, suggesting that the adsorption of acephate and trichlorfon saturated. Thus, incubation times of 20 min for acephate and 5 min for trichlorfon were chosen to gain high sensitivity and efficiency.

Calibration curves

Under the optimum conditions, the detection of various concentrations of acephate and trichlorfon were investigated with DPV using the MIP/Fe_3O_4@MWNTs-COOH/CS sensor (see inset in Fig. 6). The peak current decreased as the OP concentration increased, and the reduction in the △I for ORPS was proportional to the acephate and trichlorfon concentrations for the ranges 1.0×10^{-4}–1.0×10^{-10} M and 1.0×10^{-5}–1.0×10^{-11} M, respectively (Fig. 6). The linear calibration equation for acephate was: ΔI (μA)=4.306 log $C_{[Acephate]}$+44.347 (R^2=0.9988) and that for trichlorfon was: ΔI (μA)=5.222 log $C_{[Trichlorfon]}$+57.976 (R^2=0.9961). The imprinted sensor had a detection limit (signal/noise=3) of 6.81×10^{-11} M for acephate and 8.94×10^{-12} M for trichlorfon.

Selectivity

To verify the selectivity capacity of the MIP sensor, 1.0 mM of acephate, trichlorfon, methamidophos and omethoate solutions were detected separately. The peak current magnitudes in ORPS for acephate, trichlorfon, methamidophos and omethoate concentrations, measured with the NIP sensor were 6.53, 8.74, 5.67 and 5.05 μA, respectively. Compared with the NIP sensor, good selectivity was observed for the MIP sensor with respect to the higher peak current magnitudes of 27.57, 36.72, 24.95 and 22.76 μA, which was attributed to the specific binding sites that formed after the template was removed. Therefore, a potentially useful imprinted sensor for detecting traces of multi-pesticides was successfully fabricated.

Stability and reproducibility of the imprinted sensor

The long-term stability of the imprinted sensor was studied over a period of 30 days. The imprinted sensor maintained 93.5% of its original response after the electrode was stored for 15 days, and its response decreased to 86.3% after 30 days. The reproducibility was evaluated by detecting a 0.1 mM trichlorfon solution five times and a low RSD of 3.01% was obtained. The fabrication reproducibility was also investigated by measuring the trichlorfon solution (0.1 mM) with six different freshly imprinted sensors, giving a RSD of 4.35%. The data are shown in Table S1 and S2. These results indicated that the imprinted electrochemical sensor had good stability and reproducibility.

Application of MIP/Fe_3O_4@MWNTs-COOH/CS sensors

To evaluate the practical applicability of the developed sensor, the content of acephate or trichlorfon in the fortified kidney bean and cucumber samples was detected, respectively. The results were summarized in Table 1. Good recoveries ranging from 85.7 to 94.9% with RSDs of 3.46–5.18% were obtained. Thus, the developed imprinted sensor was promising for the accurate quantification of acephate and trichlorfon in real samples. It is known that the stabilities of acephate and trichlorfon are poor. Therefore, the recoveries are relative low, which will be improved in further study.

Conclusions

In this work, an imprinted electrochemical sensor sensitized with Fe_3O_4@MWNTs-COOH was successfully fabricated to detect acephate and trichlorfon in vegetable samples. The established MIP sensor exhibited a fast response, good sensitivity and wide linear concentration range towards acephate and trichlorfon, providing a promising screening tool for the detection of multi-pesticide residues in food safety analysis.

Acknowledgments

The authors are grateful for the financial support from the National Natural Science Foundation of China (project No. 31171699) and the Agricultural Science and Technology Achievements Transformation Project of China (project No. 2013GB2C600276).

References

1 X. N. Yan, J. Deng and J. S. Xu, *Sens. Actuators, B*, 2012, **171-172**, 1087-1094.

2 M. R. Majidi, K. Asadpour-Zeynali and M. Nazarpur, *J. Aoac Int.*, 2009, **92**, 548-554.

3 J. M. Gong, X. J. Miao, T. Zhou and L. Z. Zhang, *Talanta*, 2011, **85**, 1344-1349.

4 T. J. Mohammad, S. Mohammad and S. Hossein, *Anal. Chim. Acta*, 2014, **814**, 69-78.

5 X. P. Liu, D. K. Li, J. Q. Li, R. Gavin and J. M. Philip, *J. Hazard. Mater.*, 2013, **263**, 761-767.

6 K. Seebunrueng, Y. Santaladchaiyakit and S. Srijaranai, *Chemosphere*, 2014, **103**, 51-58.

7 C. I. Mónica, L. Z. Luis, T. C. Sagrario and M. L. Susana, *J. Chromatogr. A*, 2014, **1341**, 31-40.

8 Y. Merdassa, J. F. Liu and N. Megersa, *Talanta*, 2013, **114**, 227-234.

9 Z. Y. Sang, Y. T. Wang, Y. K. Tsoi and K. S.Y. Leung, *Food Chem.*, 2013, **136**, 710-717.

10 K. L. Lynch, A. R. Breaud, H. Vandenberghe, A. H. B. Wu and W. Clarke, *Clin. Chem. Acta*, 2010, **411**, 1474-1481.

11 W. B. Guan, Z. N. Li, H. Y. Zhang, H. J. Hong, N. Rebeyev, Y. Ye and Y. Q. Ma, *J. Chromatogr. A*, 2013, **1286**, 1-8.

12 Z. L. Xu, Q. Wang, H. T. Lei, S. A. Eremin, Y. D. Shen, H. Wang, R. C. Beier, J. Y. Yang, K. A. Maksi-mova and Y. M. Sun, *Anal. Chim. Acta*, 2011, **708**, 123-129.

13 H. R. Lee, S. M. Cho, J. Kim and D. S. Chung, *J. Chromatogr. A*, 2014, **1346**, 117-122.

14 J. W. Dong, N. Gao, Y. Peng, C. Guo, Z. Q. Lv, Y. Wang, C. H. Zhou, B. A. Ning, M. Liu and Z. X. Gao, *Food Control*, 2012, **25**, 543-549.

15 Z. C. Hu, J. J. Xu, Y. Tian, R. Peng and Y. Z. Xian, *Electrochim. Acta*, 2009, **54**, 4056-4061.

16 W. J. Lian, S. Liu, J. H. Yu, X. R. Xing, J. Li, M. Cui and J. D. Huang, *Biosens. Bioelectron.*, 2012, **38**, 163-169.

17 C. Xue, Q. Han, Y. Wang, J. H. Wu, T. T. Wen, R.Y. Wang, J. L. Hong and X. M. Zhou, *Biosens. Bioelectron.*, 2013, **49**, 199-203.

18 L. L. Zhu, Y. H. Cao and G. Q. Cao, *Biosens. Bioelectron.*, 2014, **54**, 258-261.

19 X. H. Tan, B. H. Li, K. Y. Liew and C. Y. Li, *Biosens. Bioelectron.*, 2010, **26**, 868-871.

20 Y. F. Hu, J. X. Li, Z. H. Zhang, H. B. Zhang, L. J. Luo and S. Z. Yao, *Anal. Chim. Acta*, 2011,

698, 61-68.

21 Y. K.Yang, G. Z. Fang, G. Y. Liu, M. F. Pan, X. M. Wang, L. J. Kong, X. L. He and S. Wang, *Biosens. Bioelectron.*, 2013, **47**, 475-481.

22 Z. H. Zhang, Y. F. Hu, H. B. Zhang and S. Z. Yao, *Biosens. Bioelectron.*, 2010, **26**, 696-702.

23 H. J. Chen, Z. H. Zhang, L. J. Luo and S. Z. Yao, *Sens. Actuators, B*, 2012, **163**, 76-83.

24 S. A. Kumar, S. F. Wang, C. T. Yeh, H. C. Lu, J. C. Yang and Y. T. Chang, *J. Solid State Electrochem.*, 2010, **14**, 2129-2135.

25 Z. Yao, X. M. Zhou, Z. Yang and S. M. Huang, *Biosens. Bioelectron.*, 2011, **30**, 28-34.

26 X. Y. Li, Y. X. Liu, L. C. Zheng, M. J. Dong, Z. H. Xue, X. Q. Lu and X. H. Liu, *Electrochem. Acta*, 2013, **113**, 170-175.

27 Y. Y. Sun, Q. X. Ren, X. Liu, S. Zhao and Y. Qin, *Biosens. Bioelectron.*, 2013, **39**, 289-295.

28 R. F. Chen, G. Q. Song and Y. Wei, *J. Phys. Chem.*, 2010, **114**, 13409-13413.

29 K. J. Huang, D. J. Niu, W. Z. Xie and W. Wang, *Anal. Chim. Acta*, 2010, **659**, 102-108.

30 Q. Chen, S. Ai, X. Zhu, H. Yin, Q. Ma and Y. Qiu, *Biosens. Bioelectron.*, 2009, **24**, 2991-2996.

31 J. Tkac, J. W. Whittaker and T. Ruzgas, *Biosens. Bioelectron.*, 2007, **22**, 1820-1824.

32 Q. Zhang, L. B. Wang, K. C. Ahn, Q. Sun, B. S. Hu and J. Wang, *Anal. Chim. Acta*, 2007, **596**, 303-311.

33 Z. H. Zhang, Y. F. Hu, H. B. Zhang, L. J. Luo and S. Z. Yao, *J. Colloid Interface Sci.*, 2010, **344**, 158-164.

34 L. Kong, X. F. Lu and W. J. Zhang, *J. Solid State Chem.*, 2008, **181**, 628-636.

35 N. Chauhan and C. S. Pundir, *Anal. Chim. Acta*, 2011, **701**, 66-74.

36 Y. Yong, Y. X. Bai, Y. F. Li, L. Lin, Y. J. Cui and C. G. Xia, *J. Magn. Magn. Mater.*, 2008, **320**, 2350-2355.

37 J. Liu and A. T. Harris, *Chem. Eng. Sci.*, 2009, **64**, 1511-1521.

38 Q. H. Li, Q. H. Zhou, D. Deng, Q. Z. Yu, L. Gu, K. D. Gong, K. H. Xu and T. Nonferr, *Metal. Soc.*, 2013, **23**, 1421-1427.

39 D. S. Ahmed, A. J. Haider and M. R. Mohammad, *Energy procedia*, 2013, **36**, 1111-1118.

40 C. Cunha, S. Panseri1, D. Iannazzo, A. Piperno, A. Pistone, M. Fazio, A. Russo, M. Marcacci and S. Galvagno, *Nanotech*., 2012, **23**, 265102.

Figure captions

Fig. 1 Schematic diagram of the MIP/Fe_3O_4@MWNTs-COOH/CS/GCE.

Fig. 2 (A) XRD patterns for MWNTs (a) and MWNTs-COOH (b). (B) XRD patterns for Fe_3O_4@ MWNTs-COOH (c) and Fe_3O_4 (d).

Fig. 3 TEM images of MWNTs-COOH (a) and Fe_3O_4@MWNTs-COOH (b)

Fig. 4 CVs of the electrodeposition of MIP/Fe_3O_4@MWNTs-COOH/CS/GCE at a scan rate of 50 mV s^{-1} for 10 successive cycles.

Fig. 5 (A) CV curves of the bare GCE (a), CS/GCE (b), Fe_3O_4/GCE (c), MWNTs-COOH /CS/GCE (d), Fe_3O_4@MWNTs-COOH/CS/GCE(e), MIP/Fe_3O_4@ MWNTs-COOH/CS/GCE before removing the template (f) and MIP/Fe_3O_4@MWNTs-COOH/CS/GCE after removing the template (g). (B) DPV curves of MIP/Fe_3O_4@MWNTs-COOH/CS/GCE before removing the template (h), MIP/Fe_3O_4@MWNTs-COOH/CS/GCE after removing the template (i), MIP/Fe_3O_4@MWNTs-COOH/CS/GCE incubated in 1.0 mM acephate (j) and trichlorfon (k) solutions, respectively, and NIP/Fe_3O_4@ MWNTs-COOH/CS/GCE (l).

Fig. 6 Calibration curves of MIP/Fe_3O_4@MWNTs-COOH/CS sensor used to measure acephate in a pH 5.5 PBS (A) and trichlorfon in a pH 7.5 PBS (B) containing 2 mM of ORPS (inset: DPV curves).

Table 1 Results of DPV measurements of acephate and trichlorfon in spiked vegetable samples (n=3)

Pesticides	Spiked levels ($\times 10^{-10}$ M)	Kidney bean sample		Cucumber sample	
		Found levels ($\times 10^{-10}$ M)	Recovery (%) (mean ± RSD)	Found levels ($\times 10^{-10}$ M)	Recovery (%) (mean ± RSD)
Acephate	3	2.71	90.3 ± 4.61	2.57	85.7 ± 4.94
	15	14.08	94.9 ± 3.46	13.77	91.8 ± 3.62
	30	24.36	91.2 ± 4.14	27.98	93.3 ± 4.05
Trichlorfon	0.4	0.35	87.5 ± 5.18	0.37	92.5 ± 4.32
	2	1.84	92.0 ± 4.53	1.78	89.0 ± 3.95
	4	3.63	90.8 ± 3.92	3.53	88.3 ± 4.88

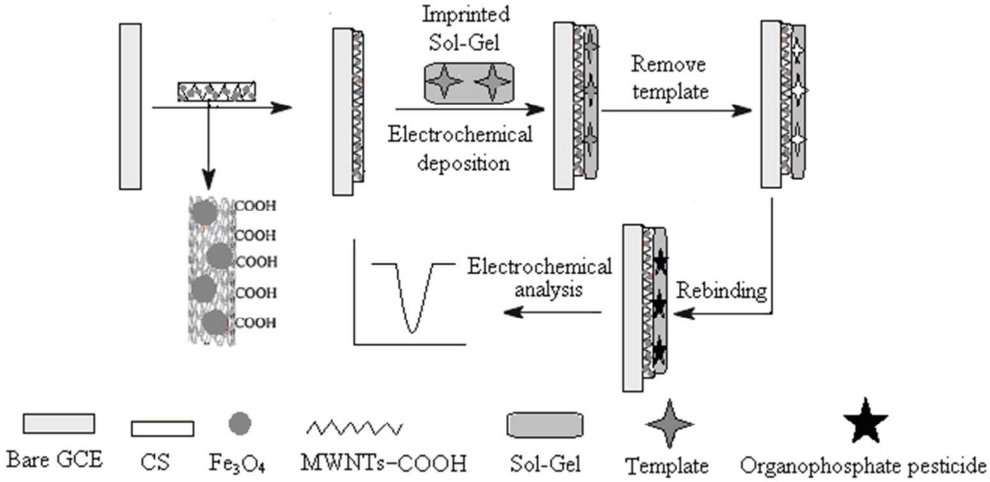

Fig. 1

56x30mm (300 x 300 DPI)

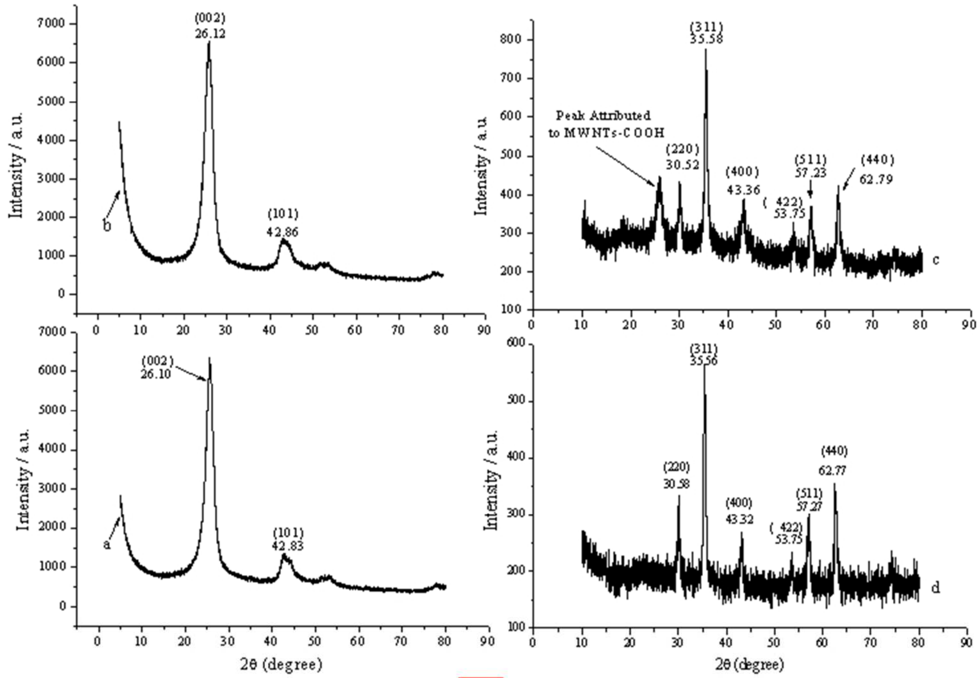

Fig. 2

199x143mm (96 x 96 DPI)

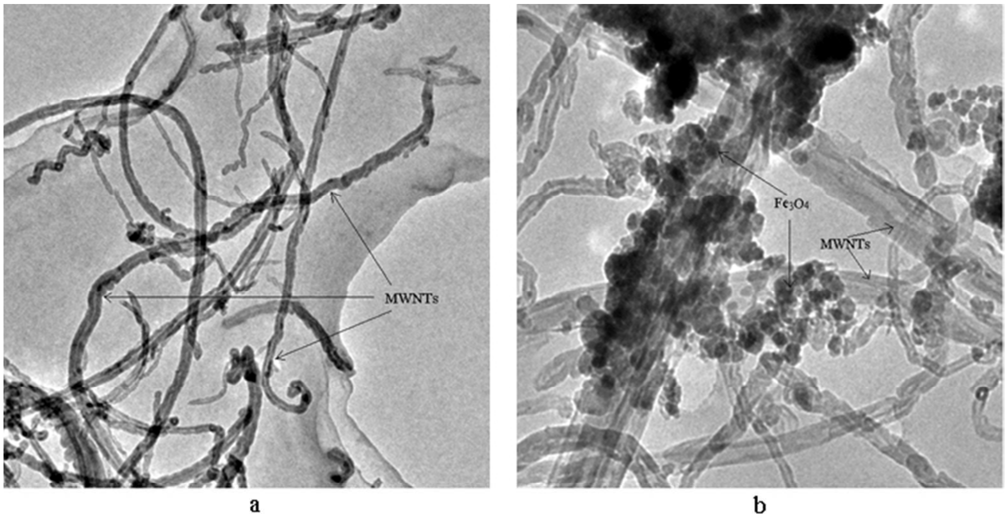

Fig. 3

196x112mm (96 x 96 DPI)

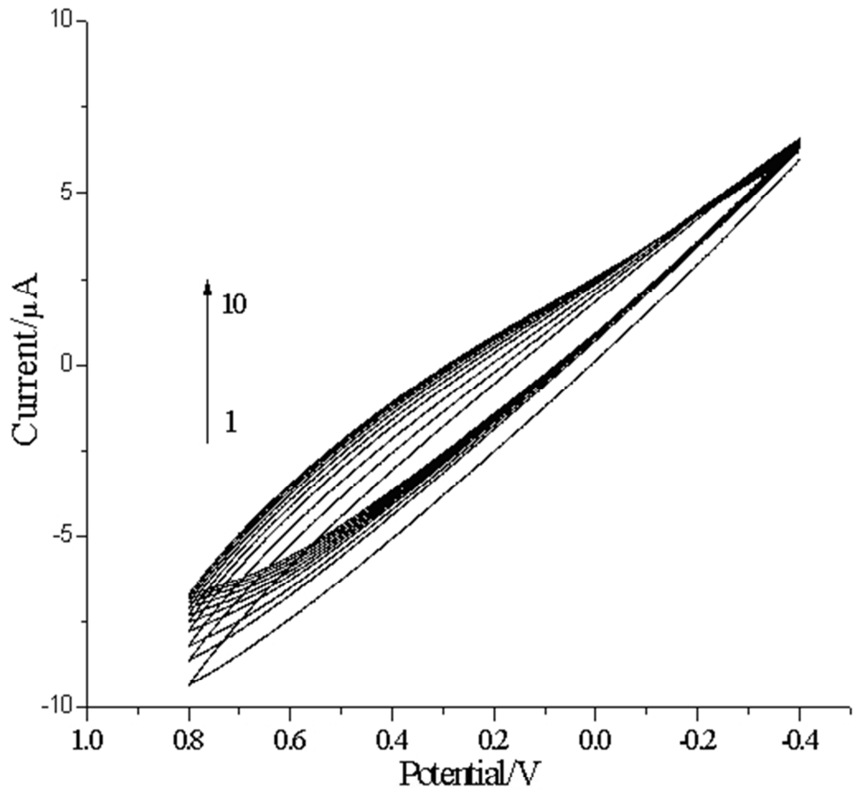

Fig. 4

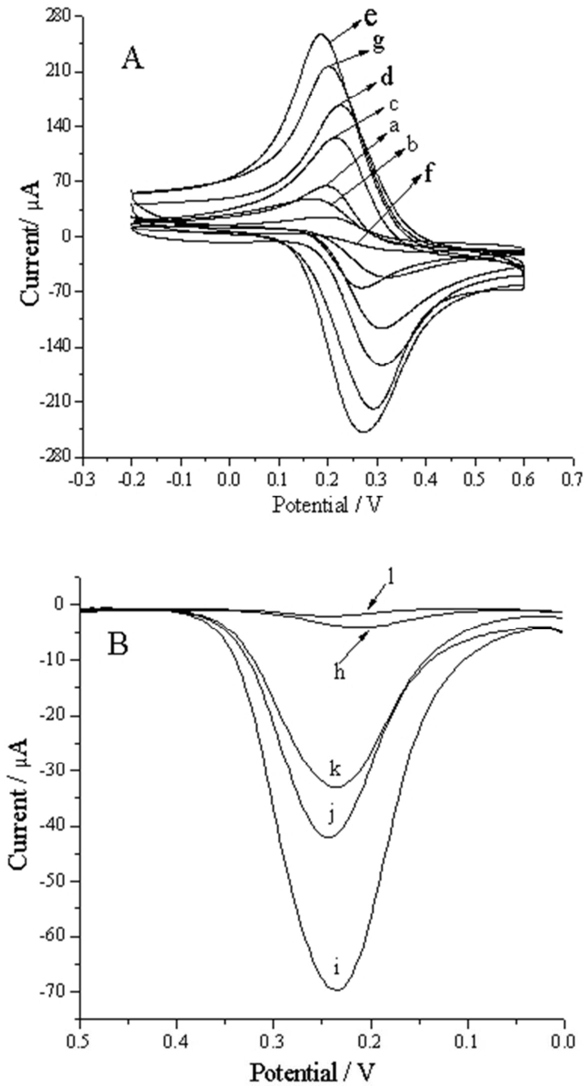
A
e
g
d
c
a
b
f
Current/ μA
Potential / V
B
l
h
k
j
i
Current / μA
Potential / V

Fig. 5

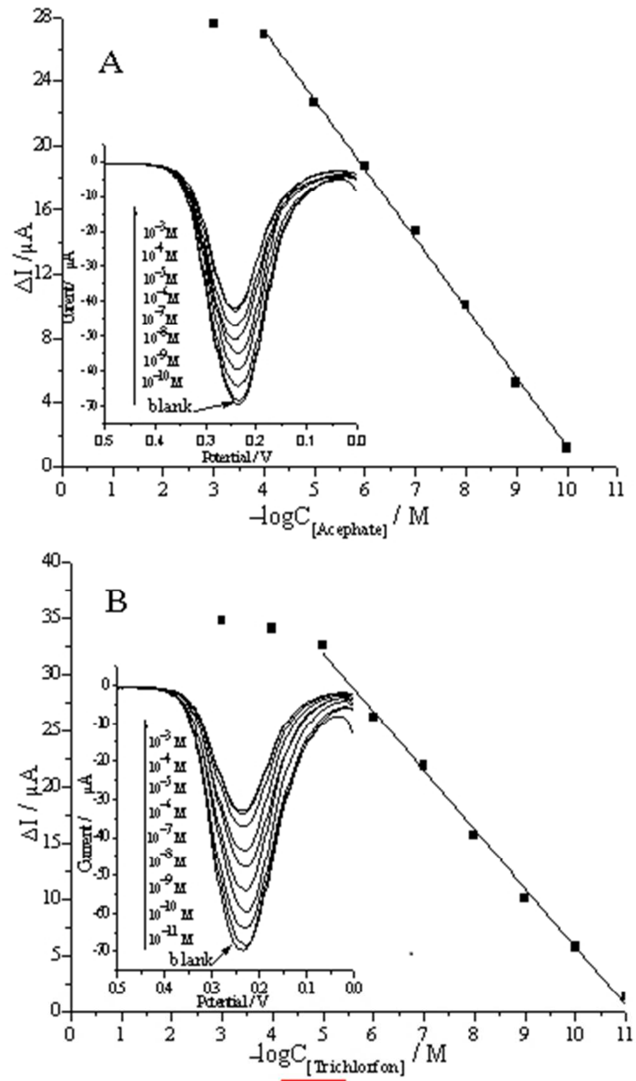

Fig. 6

113x180mm (96 x 96 DPI)